POLITECNICO DI TORINO
Repository ISTITUZIONALE

Evaluation of energy and failure parameters in composite structures via a Component-Wise approach

(Article begins on next page)

04 August 2020

Evaluation of Energy and Failure Parameters in Composite Structures via a Component-Wise Approach

M. Maiarú[*],
University of Washington, Department of Aeronautics and Astronautics Engineering
Seattle, WA, USA, mmaiaru@uw.edu

M. Petrolo[†],
Politecnico di Torino, Department of Mechanical and Aerospace Engineering
Turin, Italy, marco.petrolo@polito.it

E. Carrera[‡]
Politecnico di Torino, Department of Mechanical and Aerospace Engineering
Turin, Italy, erasmo.carrera@polito.it
Department of Mathematics, Faculty of Science, King Abdulaziz University
P.O. Box 80203, Jeddah 21589, Saudi Arabia

Final Version of Ms. No. JCOMB_2016_823

Author for correspondence:
Erasmo Carrera, Professor
Department of Mechanical and Aerospace Engineering,
Politecnico di Torino,
Corso Duca degli Abruzzi 24,
10129 Torino, Italy,
tel: +39 011 090 6836,
fax: +39 011 090 6899,
e-mail: erasmo.carrera@polito.it

---

[*]Postdoctoral Research Fellow
[†]Assistant Professor
[‡]Professor of Aerospace Structures and Aeroelasticity

Abstract

This paper deals with the static analysis of fiber reinforced composites via the Component-Wise approach (CW). The main aim of this work is the investigation of the CW capabilities for the evaluation of integral quantities such as the strain energy, or integral failure indexes. Such quantities are evaluated in the global structures and local volumes. The integral failure indexes, in particular, are proposed as alternatives to pointwise failure indexes. The CW approach has been recently developed as an extension of the 1D Carrera Unified Formulation (CUF). The CUF provides hierarchical higher-order structural models with arbitrary expansion orders. In this work, Lagrange-type polynomials are used to interpolate the displacement field over the element cross-sections. The CW makes use of the 1D CUF finite elements to model simultaneously different scale components (fiber, matrix, laminae and laminates) with a reduced computational cost. CW models do not require the homogenization of the material characteristics nor the definition of mathematical lines or surfaces. In other words, the material characteristics of each component, e.g. fibers and matrix, are employed, and the problem unknowns are placed above the physical surface of the body. In the perspective of failure analyses, the integral evaluation of failure parameters is introduced to determine critical portions of the structure where failure could take place. Integral quantities are evaluated using 3D integration sub-domains that may cover macro- and micro-volumes of the structure. The integral quantities can be evaluated directly on fiber and matrix portions. Numerical results are provided for different configurations and compared with solid finite element models. The results prove the accuracy of the CW approach and its computational efficiency. In particular, 3D local effects can be detected. The use of the integral failure index provides qualitatively reliable results; however, experimental campaigns should be carried out to related such indexes to the failure occurrence.

Keywords: Component-Wise, Composites, Carrera Unified Formulation, 1D Models.

1 Introduction

Fiber reinforced composite structures have been increasingly used in many engineering applications over the last decades. Nevertheless, many aspects of composites are still only partially understood and hard to model. A typical example being failure and fatigue processes. The proper mathematical modeling of such phenomena should take into account the multiscale properties of composites. Multiscale approaches have been recently proposed to model the different scales involved in the analysis of composites and provide a refined description of the stress and strain on the components [1, 2, 3, 4, 5].

In a failure analysis scenario, integral quantities are commonly used to predict failure. Depending on the failure mode, integrals can be evaluated on lines, areas or volumes, as shown in Fig. 1. For instance, forces exchanged through the thickness can lead to delamination. Therefore, 1D-, 2D- and 3D-sub-domains nearby the lamina interfaces can be appropriate zones to investigate. Or, if the debonding/pull-out mechanisms have to be analyzed, sub-domains around the fiber/matrix interface can be taken into account. As in Fig. 2, line contours around microcracks can be considered when the matrix behaviour has to be studied.

In the framework of the evaluation of integral parameters, the J-integral method was introduced for the analysis of metallic structure and, in the last decades, has received many attentions for its several attractive features. According to this theory [6], a path independent parameter, J, can represent an average measure of the crack tip elastic-plastic field. The J-integral can be directly evaluated from single load-displacement records [7], making this value particularly attractive to be used as a fracture criterion [8]. This method has been extensively used for two-dimensional problems, and for traditional metallic materials; an extension to three-dimensional problems can be found in [9]. The J-integral approach has then been extended to composites; it can be used to measure the crack resistance curves (R-curve) in fiber-dominated failure modes of polymer-matrix composites, and to characterize the fracture toughness. It has also been used to evaluate the parameters used in softening laws for the numerical simulation of the fracture mechanism [10]. The J-integral is a path-independent parameter that can also be used to analyze the failure areas when the linear elastic fracture mechanics approximations are not valid as shown in [11]. A similar approach was presented in [12] for cementitious composites while, in [13], it has been used to determine the fracture toughness of the tensile and compressive fiber failure modes.

The accuracy of point-wise and integral predictions are related to the accuracy of the displacement, strain, and stress fields. Accurate 3D fields in composite structures require refined models. Typical classes of refined structural models for composites are based on higher-order models [14, 15], Zig-zag theories [16, 17, 18], Layer-Wise (LW) approaches [19, 20, 21], and mixed variational approaches [22]. The present work makes use of 1D advanced structural models based on the Carrera Unified Formulation [23, 21, 24]. In particular, the Component-Wise approach (CW) is adopted. The CW stemmed from the 1D CUF. Lagrange polynomials are usually adopted to model the cross-section displacement field. In a CW model, each component of a complex structure is modeled through 1D models. 1D, 2D, and 3D structural elements can be modeled through 1D

models by enriching the displacement fields. The definition of mathematical lines and surfaces is no more needed since the unknown variables can be placed on the physical surfaces of the structure. Each component can be modeled with its material characteristics, and no homogenization is needed. CW models have been recently exploited to deal with the analysis of aerospace structures [25, 26, 27, 28, 29], civil structures [30, 31], fiber/matrix cells of composite structures [32, 33], and damage analysis [34, 35]. The use of the CW approach for composites was introduced in [32, 33]. The capability to obtain the solid-like accuracies was proved. The current work presents recent developments of the CW to evaluate integral parameters in composite structures. Particular attention was paid to the proper choice of the integration domain. Since the micro and the macro scales can be modelled simultaneously, integrals were evaluated simultaneously in a whole lamina, fiber, or matrix portion or specific parts of these components.

This work is a companion paper of [36]. In particular, this paper extends the numerical cases presented in [36] via comparisons with 3D finite elements and more comprehensive evaluations of the local effects. This paper is organized as follows: a brief theoretical introduction to the present formulation is given in Section 2. An overview of the CW and the evaluation of integral parameters is given in section 3. The numerical examples are presented and discussed in Section 4. The main conclusions are drawn in Section 5.

2   CUF 1D Formulation

Let us assume the Cartesian, orthogonal coordinate frame shown in Fig. 3. In the CUF framework, the displacement field of a 1D structural model is written as follows:

$$\mathbf{u}(x, y, z) = F_\tau(x, z)\mathbf{u}_\tau(y), \qquad \tau = 1, 2, ..., M \tag{1}$$

where $\mathbf{u}(x, y, z) = \{u_x, u_y, u_z\}^T$ is the displacement vector; $F_\tau(x, z)$ indicates the cross-section functions; $\mathbf{u}_\tau$ is the generalized displacement vector; M indicates the number of terms in the expansion. The repeated subscript indicates summation. The choice of F_τ and M is arbitrary. In other words, various types of basis functions can be used to model the displacement field across the section - e.g. polynomials, harmonics, exponentials, and combinations thereof - as well as any expansion orders.

In this paper, Lagrange polynomial expansions (LE) were used for the displacement field. Bi-quadratic nine-nodes (L9) Lagrange polynomials are used as F_τ. The displacement field within an L9 element can be written as:

$$u_x(x, y, z) = F_1(x, z)u_{x1}(y) + F_2(x, z)u_{x2}(y) + ... + F_9(x, z)u_{x9}(y)$$
$$u_y(x, y, z) = F_1(x, z)u_{y1}(y) + F_2(x, z)u_{y2}(y) + ... + F_9(x, z)u_{y9}(y) \tag{2}$$
$$u_z(x, y, z) = F_1(x, z)u_{z1}(y) + F_2(x, z)u_{z2}(y) + ... + F_9(x, z)u_{z9}(y)$$

Where $u_{x1}, ..., u_{z9}$ are the translational components of the nine points of the L9 element. The unknown variables are only pure displacements. Lagrange polynomials can be found in [24]. Multiple L-elements can

be used above a cross-section. Figure 4 shows a typical L9 distribution above a cross-section with local loads. The local refinement of the displacement field is achieved via the use of a finer discretization. Figure 5 shows the LE capability of using directly the physical surfaces of the structure to place the unknown variables. While classical models require the definition of a line - commonly known as the beam axis - along which the unknown variables are defined, LE can use the physical boundaries of the 3D body. Such a feature can be of fundamental importance whenever a 3D CAD geometry must be dealt with.

2.1 Geometrical and Constitutive Equations

The stress σ and the strain ϵ vectors are defined as follows:

$$
\boldsymbol{\sigma} = \{\sigma_{xx}, \sigma_{yy}, \sigma_{zz}, \sigma_{xy}, \sigma_{xz}, \sigma_{yz}\}^T
$$
$$
\boldsymbol{\epsilon} = \{\epsilon_{xx}, \epsilon_{yy}, \epsilon_{zz}, \epsilon_{xy}, \epsilon_{xz}, \epsilon_{yz}\}^T
$$

(3)

The linear strain-displacement relations are employed,

$$
\boldsymbol{\epsilon} = \boldsymbol{D}\boldsymbol{u}
$$

(4)

where $\boldsymbol{D}$ is

$$
\boldsymbol{D} = \begin{bmatrix} \frac{\partial}{\partial x} & 0 & 0 \\ 0 & \frac{\partial}{\partial y} & 0 \\ 0 & 0 & \frac{\partial}{\partial z} \\ \frac{\partial}{\partial y} & \frac{\partial}{\partial x} & 0 \\ \frac{\partial}{\partial z} & 0 & \frac{\partial}{\partial x} \\ 0 & \frac{\partial}{\partial z} & \frac{\partial}{\partial y} \end{bmatrix} = \begin{bmatrix} \frac{\partial}{\partial x} & 0 & 0 \\ 0 & 0 & 0 \\ 0 & 0 & \frac{\partial}{\partial z} \\ 0 & \frac{\partial}{\partial x} & 0 \\ \frac{\partial}{\partial z} & 0 & \frac{\partial}{\partial x} \\ 0 & \frac{\partial}{\partial z} & 0 \end{bmatrix} + \begin{bmatrix} 0 & 0 & 0 \\ 0 & \frac{\partial}{\partial y} & 0 \\ 0 & 0 & 0 \\ \frac{\partial}{\partial y} & 0 & 0 \\ 0 & 0 & 0 \\ 0 & 0 & \frac{\partial}{\partial y} \end{bmatrix} = [\boldsymbol{D}_\Omega] + [\boldsymbol{D}_y]
$$

(5)

The constitutive law is

$$
\boldsymbol{\sigma} = \tilde{\boldsymbol{C}}\boldsymbol{\epsilon}
$$

(6)

For the sake of brevity, the coefficients of $\tilde{\boldsymbol{C}}$ are non reported here, they can be found in [37].

2.2 Finite Element Formulation and the Fundamental Nucleus

The generalised displacement vector $\mathbf{u}_\tau$ is interpolated along the y direction by means of the shape functions N_i,

$$
\boldsymbol{u}(x, y, z) = F_\tau(x, z)N_i(y)\boldsymbol{u}_{\tau i}
$$

(7)

where $\mathbf{u}_{\tau i}$ is the nodal unknown vector. According to the principle of virtual displacements, the internal strain energy L_{int} can be written as follows:

$$\delta L_{int} = \int_V \delta \boldsymbol{\epsilon}^T \boldsymbol{\sigma} \, dV \tag{8}$$

Where δ stands for virtual variation. Considering Eqs. 4, 6 and 7, the virtual variation of the strain energy can be written in a compact form:

$$\delta L_{int} = \delta \boldsymbol{u}_{sj}^T \mathbf{K}^{\tau sij} \boldsymbol{u}_{\tau i} \tag{9}$$

where $\mathbf{K}^{\tau sij}$ is the fundamental nucleus of the stiffness matrix and the superscripts indicate the four indexes exploited to expand the elemental matrix: τ and s are related to the expansion functions F_τ and F_s whereas i and j are related to the shape functions N_i and N_j. The fundamental nucleus, which is a 3×3 array, is formally independent of the order of the beam model. By introducing the geometrical and constitutive relations, it is possible to rewrite the virtual variation of L_{int} as

$$
\begin{aligned}
\delta L_{int} = \delta \mathbf{u}_{sj}^T &\left\{ \int_V \left[\left(\boldsymbol{D}_\Omega + \boldsymbol{D}_y \right)^T \left(F_s(x,z) N_j(y) \boldsymbol{I} \right) \right] \boldsymbol{C} \left[\left(\boldsymbol{D}_\Omega + \boldsymbol{D}_y \right) \left(N_i(y) F_\tau(x,z) \boldsymbol{I} \right) \right] dV \right\} \mathbf{u}_{\tau i} = \\
= \delta \mathbf{u}_{sj}^T &\left\{ \int_l \left(N_j(y) \left(\int_\Omega \left[\boldsymbol{D}_\Omega^T \left(F_s(x,z) \boldsymbol{I} \right) \right] \boldsymbol{C} \left[\boldsymbol{D}_\Omega \left(F_\tau(x,z) \boldsymbol{I} \right) \right] d\Omega \right) N_i(y) \right) dy + \right. \\
&+ \int_l \left(N_j(y) \left(\int_\Omega \left[\boldsymbol{D}_\Omega^T \left(F_s(x,z) \boldsymbol{I} \right) \right] \boldsymbol{C} F_\tau(x,z) d\Omega \right) \boldsymbol{D}_y \left(N_i(y) \boldsymbol{I} \right) \right) dy + \\
&+ \int_l \left(\boldsymbol{D}_y^T \left(N_j(y) \boldsymbol{I} \right) \left(\int_\Omega F_s(x,z) \boldsymbol{C} \left[\boldsymbol{D}_\Omega \left(F_\tau(x,z) \boldsymbol{I} \right) \right] d\Omega \right) N_i(y) \right) dy + \\
&\left. + \int_l \left(\boldsymbol{D}_y^T \left(N_j(y) \boldsymbol{I} \right) \left(\int_\Omega F_s(x,z) \boldsymbol{C} F_\tau(x,z) d\Omega \right) \boldsymbol{D}_y \left(N_i(y) \boldsymbol{I} \right) \right) dy \right\} \mathbf{u}_{\tau i}
\end{aligned}
\tag{10}
$$

where Ω is the cross-section domain and $\mathbf{I}$ is the unit matrix. All the other finite element matrices and vectors can be written in a similar way, as shown in [24].

3 The CW approach and evaluation of integral quantities

CUF 1D models can be particularly convenient in the case of multi-component structures. Typical examples are aircraft wings and composite structures. These structures are composed of multiple components, which can have rather different geometrical and material characteristics. A fibre reinforced composite plate is made of layers made of matrix and fibers. Usually, such plates are modeled as homogenized structures through the equivalent single layer (ESL) and layer-wise (LW) approaches. The ESL models a multilayered plate as an equivalent monolayer plate. The LW retains each layer but with higher computational costs. The CW approach can be seen as a further improvement of the previous techniques that allows the modelling of a fiber-reinforced composite structure up to the component scale.

The CW exploits LE 1D elements to model each component of a structure separately and independently of their geometrical and material characteristics. Each 1D, 2D, 3D or micro and macro component can be modeled via LE 1D models with no need for ad hoc coupling and interface techniques. Figure 6 shows a typical CW strategy for a composite plate; 1D LE models can be simultaneously adopted to model layers (macroscale), matrix and fibres (microscale). This methodology can be very powerful when, for instance, detailed stress fields are required in a specific portion of the structure. It is important to underline that each component geometrical and material characteristics are retained, and the CW approach does not require coupling techniques, as the FE matrices of each element are formally the same. Figure 7 shows the different assemblage strategies for a multicomponent structure stiffness matrix. In classical approaches, the structure is reduced to a single equivalent structure. In the CW, the stiffness matrix elements of different components are superimposed only at the interface level to impose the displacement continuity. CW models can be locally refined by using higher- or lower-order models where required. Such a feature leads to further computational cost reductions.

Previous works have evidenced the enhanced capabilities of the CW to detect complete 3D, accurate displacement/strain/stress and failure index fields in the matrix, fibers, layers and interfaces of composite structures with low computational costs [33, 32].

3.1 Integral quantities

The present paper focuses on the evaluation of integral quantities, such as the strain energy, in global and local portions of the structure. Given the 3D geometry of the structure, some sub-volumes, V_i, are considered. The strain energy in V_i can be calculated as follows:

$$E_i = \int_{V_i} \boldsymbol{\sigma}^T \boldsymbol{\epsilon} \ dV_i \tag{11}$$

In particular, the contributions from the axial and shear strains are given by

$$E_{i,ax} = \int_{V_i} \sigma_{yy}\epsilon_{yy} \ dV_i, \qquad E_{i,s} = \int_{V_i} (\sigma_{yz}\epsilon_{yz} + \sigma_{xy}\epsilon_{xy}) \ dV_i \tag{12}$$

In composite structures, several failure mechanisms can take place, such as fiber or matrix collapse, debonding or delamination. To determine where failure may occur, integral quantities can be evaluated in sub-domains that can be lines, areas or volumes of the components, or at lamina/fiber-matrix interfaces. Integral quantities are usually computed through stress and strain distributions. Therefore, the accuracy of such quantities depends on the accuracy of the strain and stress field. However, the accurate evaluation of the 3D fields can be quite cumbersome. The use of the CW may be helpful to compute these integrals with high accuracy and low computational costs. Figure 8 shows a typical analysis scenario involving a composite plate. Various sub-volume distributions are shown ranging from macro areas, e.g. entire layers, to micro areas, e.g. portions

of the matrix. The CW can predict 3D stress fields up to the micro scale and, therefore, provide reliable evaluations with no significant computational cost penalties.

One of the most common methods to predict failure in composites relies on the use of failure indexes (FI). FI offer punctual evaluations of the criticality in a given structure. However, as it is well known, FEs may be inaccurate as far as punctual evaluations are concerned. Such a problem is usually worsened by geometrical and mechanical boundary conditions. Moreover, most of the FE models require the use of homogenized, equivalent elements whose materials properties are computed from those of the single constituents, e.g. fibers and matrix. This, for instance, may lead to failure predictions that do not take into account the different properties and failure mechanisms of fibers and matrix. A possible way to overcome such a shortcoming may be represented by solid models, but with a considerable growth of the computational cost. In this paper, integral evaluations of FI are proposed and evaluated through the CW approach to avoid punctual evaluations. The aim is to highlight the capability of CW in the evaluations of failure related quantities by retaining the geometrical, and material characteristics of a fiber reinforced composite structure constituents, i.e. fibers and matrix cells. The effectiveness of such novel integral quantities to predict failure should be evaluated through experimental campaigns that are beyond the scope of this paper.

The integral version of FI within a sub-volume V_i is given by

$$FI_i^* = \frac{\int_{V_i} FI \ dV_i}{V_i} \tag{13}$$

Where FI can be one of the indexes commonly used in literature or commercial codes. In the case of multiple sub-volumes a mean value of FI* may be computed as

$$FI^* = \frac{\sum_{i=1}^{N_{Vol}} FI_i^*}{N_{Vol}} \tag{14}$$

Where N_{Vol} indicates the number of sub-volumes.

3.2 Failure indexes

In this paper, the Maximum Stress (MS) and Tsai-Wu (TW) criteria were considered as FI. For an anisotropic material, the conditions for the Maximum Stress criterion are [37]

$$
\begin{aligned}
\sigma_{11} \geq 0 &\Rightarrow \sigma_{11} \geq X_T \text{ or } \sigma_{11} < 0 \Rightarrow \sigma_{11} \leq X_C \\
\sigma_{22} \geq 0 &\Rightarrow \sigma_{22} \geq Y_T \text{ or } \sigma_{22} < 0 \Rightarrow \sigma_{22} \leq Y_C \\
\sigma_{33} \geq 0 &\Rightarrow \sigma_{33} \geq Z_T \text{ or } \sigma_{33} < 0 \Rightarrow \sigma_{22} \leq Z_C \\
\tau_{12} &\geq S_{12}; \ \tau_{13} \geq S_{13}; \ \tau_{23} \geq S_{23}
\end{aligned}
\tag{15}
$$

The Failure Coefficient, FC, for an anisotropic material changes depending on the direction. In agreement with the choice to use isotropic materials, the FC can be X or S for the Maximum Stress criterion where X is the material strength in axial directions and S, the material strength in shear directions. T and C indicate tension and compression, respectively. For the Maximum Stress criterion the FI is

$$FI = \max \left[\frac{\sigma_{ij}}{FC^{T,C,L}} \right] \tag{16}$$

Points in which the index becomes greater or equal to one indicate the failure. Table 1 shows the maximum stress values adopted for the numerical examples.

The Tsai-Wu (TW) is a quadratic interaction tensor polynomial failure criterion and can be defined as [38]

$$A_{11}\sigma_{11}^2 + A_{22}\sigma_{22}^2 + A_{33}\sigma_{33}^2 + B_1\sigma_{11} + B_2\sigma_{22} + B_3\sigma_{33} + 2A_{12}\sigma_{11}\sigma_{22} + $$
$$2A_{13}\sigma_{11}\sigma_{33} + 2A_{23}\sigma_{22}\sigma_{33} + A_{66}\tau_{12}^2 + A_{55}\tau_{13}^2 + A_{44}\tau_{23}^2 \geq 1 \tag{17}$$

Where

$$A_{11} = \frac{1}{X_T X_C} \quad A_{22} = \frac{1}{Y_T Y_C} \quad A_{33} = \frac{1}{Z_T Z_C}$$
$$B_1 = \frac{1}{X_T} - \frac{1}{X_C} \quad B_2 = \frac{1}{Y_T} - \frac{1}{Y_C} \quad B_3 = \frac{1}{Z_T} - \frac{1}{Z_C}$$
$$A_{12} = \frac{1}{2\sqrt{X_T X_C Y_T Y_C}} \quad A_{13} = \frac{1}{2\sqrt{X_T X_C Z_T Z_C}} \quad A_{23} = \frac{1}{2\sqrt{Y_T Y_C Z_T Z_C}}$$
$$A_{44} = A_{55} = A_{66} = \frac{1}{S_L S_L} \tag{18}$$

4   Numerical results

A homogeneous beam was considered as first assessment. Then, a single fiber-matrix cell was analysed. Last, a multilayered beam was considered in which various fiber-matrix cells were included. Material properties are shown in Table 1. Three isotropic materials were used. The first one was adopted in the homogeneous case and for layers. The other two materials were used to model fibers and matrix, respectively. For each material, failure coefficients are reported for tension, compression, and shear. The aim of the following numerical examples is to evaluate the capabilities of the CW models in the evaluation of integral quantities in fiber/matrix cells, with particular attention given to local effects. The choice of the loading and geometrical characteristics was carried out to shed light on these aspects. The analysis of more realistic cases should be a task for future developments. In fact, such CW cells could be used as Representative Unit Cells in multiscale analyses or used as local, micro refinements in complex macro structures.

The results were validated in terms of strain energies via 3D finite element models from commercial codes. A detailed validation campaign related to FI fields was carried out in [32].

4.1 Homogeneous beam

As a preliminary assessment, a homogeneous cell was considered as a cantilever beam, and MAT 1 used. The length of the beam is 1 mm. The cross-section is square; the height is 0.1 mm. The CW model has one L9 element above the cross-section. A solid model was used for comparison purposes, and 20-nodes element were used. Figure 9 shows the CW and solid models. Four forces were applied on the free tip of the beam, $F_1 = F_2 = F_3 = F_4 = 0.025$ N. Ten, equally long sub-volumes were considered along the axis of the beam. Table 2 shows the strain energy in each sub-volume and the total energy. The first column provides the CW model results, whereas the second column shows the results from the solid model. The results suggest that

- Perfect agreement was found between the two models. The agreement is good at global and local level. In fact, the total strain energy and the energies of each sub-volumes matched perfectly.

- The total amount of DOFs of the 1D models is three times smaller than the solid model.

- As expected, the distribution of the strain energy has a maximum in the proximity of the clamped region.

4.2 Single cell

This section deals with the analysis of a fiber/matrix cell. The cross-section is square, h = 0.1 mm, and L/h = 10 where L is the longitudinal length of the structure and h is the cross-section height. The fiber diameter (d) is 0.08 mm. 20 L9 elements were used along the cross-section. The structure is clamped at y = 0. Two loading configurations were considered, as shown in Figure 10. In a first case study, four bending force were applied at the free tip, cell corners, F = 0.025 N each. Then, pure torsion was considered using two opposite forces, F = 0.05 N, at [-h/2, L, 0] and [h/2, L, 0].

First, analogously to the previous section, two and five sub-volumes along the beam axis were considered. Table 3 shows the results regarding strain energy. E indicates the total strain energy, E_{ax} indicates the axial strain energy, and E_s the shear energy. The subscript i was used to indicate the energy in the i-th sub-volume. Bold characters indicate the maximum value of energy. Table 4 shows the energy distributions along the fiber and matrix portions of each sub-volume for the bending case. The torsion case is shown in Table 5. Table 6 shows the integral failure indexes computed via the Maximum Stress and Tsai-Wu criteria. Failure index distributions for both criteria at the clamped cross-section are shown in Fig. 11 for the bending case.

Another volume subdivision was considered and focused on the matrix in the proximity of the free tip of the beam, as shown in Fig. 12. Volumes 1-8 were placed from 0.8 to 0.9 mm, whereas 9-16 were placed along the last 10% of the beam length. Table 7 shows the results in terms of ratios between the strain energy of a given sub-volume and the strain energy in all the matrix region along the last 20% of the beam. Moreover, the integral failure index is reported. The results suggest the following:

- The local effects on the energy distributions can be evaluated via the present CW modeling.

- Local effects due to mechanical and geometrical boundary conditions influence the strain distribution. However, the influence on shear terms is much greater than on axial terms.

- The presence of point forces causes peaks of strain energy in the matrix cells. Although it must be underlined how the present structural and loading configurations are not necessarily realistic, the present analysis shows the capabilities of the CW in the prediction of local effects. Such effects can be accurately predicted along the axis and above the cross-section.

- The proposed integral failure index can qualitatively identify those areas with major stress and strain distributions. However, an appropriate choice of the sub-volume distributions is required. In particular, distributions above the cross-section involving single components should be preferred. Such a choice enables the accurate evaluation of local effects and the avoidance of homogenization of material properties.

- The quantitative interpretation of the integral failure index remains an open issue. In fact, the results suggest that there is no correspondence between the numerical values of the point-wise indexes and the integral ones.

4.3 Laminated structure

This section deals with a more complex configuration with three layers. The beam is cantilevered, and the stacking sequence is [0/90/0]. The height (h) and the width (b) are 0.6 mm and 0.8 mm, respectively; L/h = 10. Each layer is 0.2 mm thick. Figures 13, 14 show the first CW model adopted. A fiber/matrix cell was inserted into the bottom layer. The cell cross-sectional dimensions are like those of the previous section. The cell center is at $\frac{11b}{16}$. Two loading cases were considered. The bending case is given by a force, F = 5 N, applied at the free tip cross-section center. The torsion case has four forces, 1 N each, applied at the free tip cross-section corners.

Table 8 presents the total strain energy computed via the present CW model and a solid model. DOFs of each model are shown as well. Table 9 shows the strain energy in each layer and the entire beam. Table 10 reports the strain energy in the fiber/matrix cell. In particular, the fiber and matrix energy shares are given. Table 11 shows the integral failure indexes in the cell. The maximum stress criterion was used.

A second CW model was then considered as shown in Fig. 15. Eight fiber/matrix cells were considered along the bottom layer of the beam. The bending loading case was considered. Table 12 presents the total strain energy computed via the present CW model and a solid model. DOFs of each model are shown as well. Table 13 shows the strain energy in each lamina and the entire laminate. Furthermore, the contributions from the axial and shear terms are given. Table 14 focuses on the eight fiber/matrix cells. The strain energy is given for each fiber and all the matrix. Table 15 shows the integral failure index in each fiber and matrix cells. The results suggest the following:

11

- A good match between the CW models and the solid models was found. The CW DOFs are some ten times fewer than those of the solid model.

- As expected, the outer, zero degree layers have the highest shares of the strain energies due to the axial terms. Shear terms are predominant in the inner layer in the case of bending load. As far as torsion is concerned, shear contributions are predominant and equally distributed between layers.

- The CW modeling of the single fiber/cell matrix has highlighted the different energy share mechanism between fiber and matrix. As expected, fibers dominate the energy absorption in bending. Whereas, the matrix has a predominant role for shear and in torsion.

- As in the previous case, the integral failure index provides a qualitative estimation of the most critical areas of the structure.

5   Conclusions

This paper has presented results on the static analysis of fiber-reinforced composite structures via the Component-Wise approach (CW). The CW formulation, derived through the 1D Carrera Unified Formulation (CUF) structural models, can be used to model laminates, laminae, fibers and matrices separately; that is, different scale components can be modeled by using the same 1D formulation. Single fiber-matrix cells and layered structures have been considered, and the results evaluated in terms of integral quantities, such as strain energy and integral failure indexes. Comparisons with solid finite element models have been provided. Global and local effects were evaluated.
Numerical results suggest that:

- The CW results match solid model ones with good accuracy but lower computation costs. In fact, the total amount of DOFs of the 1D models is about three to four times smaller than the solid model.

- The CW can detect 3D local effects. Moreover, the avoidance of homogenization techniques enhances the prediction capabilities of the CW models at the fiber and matrix level.

- Integral failure indexes can qualitatively identify those areas with major stress and strain distributions. However, an appropriate choice of the sub-volume distributions is required. In particular, distributions above the cross-section involving single components should be preferred. Such a choice enables the accurate evaluation of local effects and the avoidance of homogenization of material properties. The quantitative interpretation of the integral failure index remains an open issue. In fact, the results suggest that there is no correspondence between the numerical values of the point-wise indexes and the integral ones.

- CW models can be used to model single cells are Repetitive Unit Cells or to model entire portions of the structure up to the micro level.

Future extensions should deal with the analysis of more complex structures, the extension to progressive failure analysis, and impact problems.

References

[1] G. Lu and E. Kaxiras. *Handbook of Theoretical and Computational Nanotechnology*, volume X. American Scientific Publishers, 2005.

[2] J. LLorca, C. González, J. M. Molina-Aldareguía, J. Segurado, R. Seltzer, F. Sket, M. Rodríguez, S. Sádaba, R. Muñoz, and L. P. Canal. Multiscale modeling of composite materials: a roadmap towards virtual testing. *Advanced Materials*, 23:5130–5147, 2011.

[3] J. Aboudi. *Mechanics of Composite Materials: A Unified Micromechanical Approach.* Elsevier, 1991.

[4] J. Aboudi. Micromechanical analysis of thermo-lnelastic multiphase short-fiber composites. *Composites Engineering*, pages 839–850, 1994.

[5] E.J Pineda, A.M. Waas, B.A. Bednarcyk, C.S. Collier, and Yarrington P.W. Progressive damage and failure modeling in notched laminated fiber reinforced composites. *International Journal of Fracture*, 158(2):125–143, 2009.

[6] J. Rice. A path independent integral and the approximate analysis of strain concentrations by notches and cracks. *Journal of Applied Mechanics*, 35:379–386, 1968.

[7] Rice, J. R. Paris, P. C. Merkle, and J. G. Some further results of j-integral analysis and estimates. *ASTM special technical publication*, 536:231–245, 1973.

[8] J. D. Begley, J.A. Landes. The j integral as a fracture criterion. *Fracture Toughness, Proceeding of the 1971 National Symposium on Fracture Mechanics, Part II, ASTM STP 514, American Society for Testing and Materials*, 35:1–20, 1972.

[9] Kishimoto, K Aoki, S Sakata, and M. On the path independent integral - j. *Engineering Fracture Mechanics*, 13:841–850, 1980.

[10] Catalanotti, G. Camanho, P.P. Xavier, J. D'avila, C.G. Marques, and A.T. Measurement of resistance curves in the longitudinal failure of composites using digital image correlation. *Composites Science and Technology*, 70:1986–1993, 2010.

[11] T. K. Sørensena, B. F. Jacobsenb. Determination of cohesive laws by the j integral approach. *Engineering Fracture Mechanics*, 70:1841–1858, 2003.

[12] R. J. Li, V. C. Ward. A novel testing technique for post-peak tensile behaviour of cementitious materials. *Fracture Toughness and Fracture Energy*, 1989.

[13] Pinho, S.T. Robinson, P. Iannucci, and L. Fracture toughness of the tensile and compressive fibre failure modes in laminated composites. *Composites Science and Technology*, 66:2069–2079, 2006.

[14] T. Kant and B. S. Manjunath. Refined theories for composite and sandwich beams with C^0 finite elements. *Computers and Structures*, 33(3):755–764, 1989.

[15] K. Kapania and S. Raciti. Recent advances in analysis of laminated beams and plates, part I: Shear effects and buckling. *AIAA Journal*, 27(7):923–935, 1989.

[16] S.G Lekhnitskii. Strength calculation of composite beams. *Vestnik inzhen i tekhnikov*, 9, 1935.

[17] S.A. Ambartsumian. Contributions to the theory of anisotropic layered shells. *Applied Mechanics Review*, 15:245–249, 1962.

[18] E. Carrera. Historical review of zig-zag theories for multilayered plates and shells. *Applied Mechanics Review*, 56(3):287–308, 2003.

[19] D.H. Robbins Jr. and J.N. Reddy. Modeling of thick composites using a layer-wise theory. *International Journal of Numerical Methods in Engineering*, 36:655–677, 1993.

[20] E. Carrera. Evaluation of layer-wise mixed theories for laminated plates analysis. *AIAA Journal*, 36:830–839, 1998.

[21] E. Carrera and M. Petrolo. Refined one-dimensional formulations for laminated structure analysis. *AIAA Journal*, 50(1):176–189, 2012. doi: 10.2514/1.J051219.

[22] E. Reissner. On a certain mixed variational theory and a proposed application. *International Journal of Numerical Methods in Engineering*, 20:1366–1368, 1984.

[23] E. Carrera and M. Petrolo. Refined beam elements with only displacement variables and plate/shell capabilities. *Meccanica*, 47:537–556, 2012.

[24] E. Carrera, M. Cinefra, M. Petrolo, and E. Zappino. *Finite Element Analysis of Structures through Unified Formulation*. John Wiley & Sons, 2014.

[25] E. Carrera, A. Pagani, and M. Petrolo. Classical, refined and component-wise theories for static analysis of reinforced-shell wing structures. *AIAA Journal*, 51(5):1255–1268, 2013.

[26] E. Carrera, A. Pagani, and M. Petrolo. Component-wise method applied to vibration of wing structures. *Journal of Applied Mechanics*, 80(4):art.no. 041012, 2013.

[27] E. Carrera and A. Pagani. Accurate response of wing structures to free-vibration, load factors, and nonstructural masses. *AIAA Journal*, 54(1):227–241, 2016.

[28] A. Pagani, M. Petrolo, E. Carrera, and G. Colonna. Dynamic response of aerospace structures by means of refined beam theories. *Aerospace Science and Technology*, 46:360373, 2015.

[29] E. Carrera and E. Zappino. Carrera Unified Formulation for free-vibration analysis of aircraft structures. *AIAA Journal*, 54(1):280–292, 2016.

[30] E. Carrera, A. Pagani, and M. Petrolo. Refined 1D finite elements for the analysis of secondary, primary and complete civil engineering structures. *Journal of Structural Engineering*, 141(4), 2015.

[31] E. Carrera and A. Pagani. Free vibration analysis of civil engineering structures by component-wise models. *Journal of Sound and Vibration*, 333(19):4597–4620, 2014.

[32] E. Carrera, M. Maiarú, and M. Petrolo. A refined 1D element for structural analysis of single and multiple fiber/matrix cells. *Composite Structures*, 96:455–468, 2013.

[33] E. Carrera, M. Maiarú, and M. Petrolo. Component-wise analysis of laminated anisotropic composites. *International Journal of Solids and Structures*, 49(13):1839–1851, 2012.

[34] M. Petrolo, E. Carrera, and A. Alawami. Free vibration analysis of damaged beams via refined models. *Advances in Aircraft and Spacecraft Sciences*, 3(1):95–112, 2016.

[35] E. Carrera, A. Pagani, and M. Petrolo. Free vibrations of damaged aircraft structures by component-wise analysis. *AIAA Journal*, 54(10):3091–3106, 2016.

[36] E. Carrera, M. Maiarú, and M. Petrolo. Evaluation of failure parameters in composite structures by component-wise approach. In *Proceedings of 54th AIAA/ASME/ASCE/AHS/ASC Structures, Structural Dynamics, and Materials Conference, Structures, Structural Dynamics, and Materials and Co-located Conferences, (AIAA 2013-1541)*, 2013. doi: 10.2514/6.2013-1541.

[37] J. N. Reddy. *Mechanics of laminated composite plates and shells. Theory and Analysis*. CRC Press, 2nd edition, 2004.

[38] S.W. Tsai and E.M. Wu. A general theory of strength for anisotropic materials. *Journal of Composite Materials*, 5(1):58–80, 1971.

Tables

	MAT 1	MAT 2	MAT 3
	Material Properties		
E (GPa)	127.6	250.6	3.252
ν [-]	0.3	0.2456	0.355
	Maximum Stress (MPa)		
X^T	1730	3398.1	66.5
X^C	1045	2052.6	255
S^L	95.1	186.8	74

Table 1: Material properties and failure coefficients.

	$E \times 10^4$ mJ	
Vol	CW	Solid
1	1.030	1.023
2	0.853	0.854
3	0.665	0.665
4	0.500	0.500
5	0.359	0.360
6	0.242	0.242
7	0.148	0.148
8	0.077	0.077
9	0.030	0.030
10	0.013	0.015
Tot	3.917	3.914
DOFs	1647	4557

Table 2: Strain energy distribution along the sub-volumes of the homogenous beam.

	Bending			Torsion	
Vol	E_i/E	$E_{ax,i}/E_{ax}$	$E_{s,i}/E_s$	E_i/E	$E_{s,i}/E_s$
1/2	0.846	0.874	0.308	0.138	0.415
2/2	0.154	0.126	0.692	0.862	0.585
1/5	0.469	0.484	0.177	0.055	0.168
2/5	0.289	0.298	0.089	0.055	0.166
3/5	0.149	0.153	0.082	0.055	0.163
4/5	0.055	0.056	0.083	0.056	0.169
5/5	0.038	0.008	0.568	0.778	0.334
	$E \times 10^3$ mJ	$E_{ax} \times 10^3$ mJ	$E_s \times 10^5$ mJ	$E \times 10^4$ mJ	$E_s \times 10^5$ mJ
Total	3.448	3.331	3.257	1.150	3.775

Table 3: Strain energy in beam sub-volumes, single cell.

	Fiber			Matrix		
Vol	E_i^f/E^f	$E_{ax,i}^f/E_{ax}^f$	$E_{s,i}^f/E_s^f$	E_i^m/E^m	$E_{ax,i}^m/E_{ax}^m$	$E_{s,i}^m/E^m$
1/2	0.873	0.874	0.591	0.509	0.872	0.046
2/2	0.127	0.126	0.409	0.491	0.128	0.954
1/5	0.483	0.484	0.326	0.275	0.488	0.039
2/5	0.298	0.298	0.180	0.171	0.293	0.005
3/5	0.153	0.153	0.167	0.088	0.151	0.004
4/5	0.057	0.056	0.164	0.033	0.056	0.008
5/5	0.009	0.008	0.162	0.423	0.012	0.945
	$E^f \times 10^3$ mJ	$E_{ax}^f \times 10^3$ mJ	$E_s^f \times 10^5$ mJ	$E^m \times 10^4$ mJ	$E_{ax}^m \times 10^4$ mJ	$E_s^m \times 10^5$ mJ
Total	3.201	3.186	1.569	2.468	1.449	1.688

Table 4: Strain energy in fiber and matrix sub-volumes, single cell, bending.

	Fiber		Matrix	
Vol	E_i^f/E^f	$E_{s,i}^f/E_s^f$	E_i^m/E^m	$E_{s,i}^m/E_s^m$
1/2	0.501	0.506	0.006	0.042
2/2	0.499	0.494	0.994	0.958
1/5	0.200	0.202	0.002	0.028
2/5	0.200	0.203	0.002	0.014
3/5	0.200	0.203	0.002	0.000
4/5	0.200	0.202	0.003	0.032
5/5	0.199	0.190	0.989	0.925
Total	$E^f \times 10^5$ mJ	$E_s^f \times 10^5$ mJ	$E^m \times 10^5$ mJ	$E_s^m \times 10^6$ mJ
	3.069	3.035	8.436	7.399

Table 5: Strain energy in fiber and matrix sub-volumes, single cell, torsion.

| | Bending | | | | Torsion | | | |
| | Fiber | | Matrix | | Fiber | | Matrix | |
Vol	FI* TW	FI* MS	FI* TW	FI* MS	FI* TW	FI* MS	FI* TW	FI* MS
	0.070	0.124	0.010	0.050	0.073	0.095	0.008	0.009
1/2	0.097	0.163	0.006	0.063	0.074	0.096	0.000	0.003
2/2	0.044	0.086	0.014	0.036	0.073	0.094	0.016	0.014
1/5	0.129	0.190	0.007	0.077	0.074	0.096	0.000	0.003
2/5	0.082	0.153	0.006	0.058	0.074	0.096	0.000	0.003
3/5	0.058	0.119	0.003	0.042	0.074	0.096	0.000	0.003
4/5	0.043	0.089	0.001	0.025	0.074	0.096	0.000	0.004
5/5	0.039	0.069	0.032	0.046	0.072	0.092	0.041	0.029

Table 6: Integral failure indexes, single cell.

| | Bending | | | Torsion | | |
Vol ID	E_i^m/E^m	$E_{s,i}^m/E^m$	FI* MS	E_i^m/E^m	$E_{s,i}^m/E^m$	FI* MS
1	0.004	0.006	0.030	0.000	0.003	0.012
2	0.004	0.006	0.030	0.000	0.003	0.011
3	0.003	0.003	0.027	0.006	0.014	0.035
4	0.003	0.003	0.045	0.006	0.014	0.032
5	0.004	0.006	0.065	0.000	0.003	0.012
6	0.004	0.006	0.065	0.000	0.003	0.011
7	0.003	0.003	0.045	0.006	0.014	0.035
8	0.003	0.003	0.027	0.006	0.014	0.032
9	0.079	0.123	0.140	0.003	0.013	0.029
10	0.079	0.123	0.140	0.003	0.013	0.030
11	0.164	0.117	0.294	0.241	0.220	0.246
12	0.164	0.117	0.163	0.241	0.220	0.190
13	0.079	0.123	0.166	0.003	0.013	0.029
14	0.079	0.123	0.166	0.003	0.013	0.030
15	0.164	0.117	0.163	0.241	0.220	0.246
16	0.164	0.117	0.294	0.241	0.220	0.190

Table 7: Local effects on matrix, single cell.

Model	$E \times 10^1$ mJ	DOFs
CW	5.798	17202
Solid	5.946	155403

Table 8: Strain energy for the laminated beam with one fiber/matrix cell via the CW and a solid model.

| | Bending | | | Torsion | | |
Lamina	E_i/E	$E_{ax,i}/E_{ax}$	$E_{s,i}/E_s$	E_i/E	$E_{ax,i}/E_{ax}$	$E_{s,i}/E_s$
1	0.451	0.499	0.116	0.353	0.508	0.319
2	0.099	0.003	0.772	0.302	0.021	0.358
3	0.450	0.499	0.113	0.345	0.471	0.323
	$E \times 10^1$ mJ	$E_{ax} \times 10^1$ mJ	$E_s \times 10^2$ mJ	$E \times 10^2$ mJ	$E_{ax} \times 10^4$ mJ	$E_s \times 10^2$ mJ
Total	5.798	5.077	6.833	7.330	9.671	6.071

Table 9: Strain energy in each layer of the laminated beam.

	Bending			Torsion		
	E_i/E	$E_{ax,i}/E_{ax}$	$E_{s,i}/E_s$	E_i/E	$E_{ax,i}/E_{ax}$	$E_{s,i}/E_s$
Matrix	0.026	0.015	0.741	0.875	0.008	0.883
Fiber	0.974	0.985	0.259	0.125	0.992	0.117
	$E \times 10^2$ mJ	$E_{ax} \times 10^2$ mJ	$E_s \times 10^4$ mJ	$E \times 10^3$ mJ	$E_{ax} \times 10^5$ mJ	$E_s \times 10^3$ mJ
Total	2.322	2.289	3.432	2.582	2.977	2.515

Table 10: Strain energy distribution in the fiber/matrix cell in the laminated beam.

	FI* - MS	
	Bending	Torsion
Matrix	0.055	0.147
Fiber	0.266	0.190
Cell	0.182	0.173

Table 11: Integral failure index over the fiber, matrix and entire cell.

Model	$E \times 10^1$ mJ	DOFs
CW	5.949	21033
Solid	6.004	386085

Table 12: Strain energy for the laminated beam with eight fiber/matrix cells via the CW and a solid model.

Lamina	E_i/E	$E_{ax,i}/E_{ax}$	$E_{s,i}/E_s$
1	0.462	0.493	0.295
2	0.096	0.003	0.610
3	0.442	0.504	0.095
	$E \times 10^1$ mJ	$E_{ax} \times 10^1$ mJ	$E_s \times 10^2$ mJ
Total	5.949	5.052	8.616

Table 13: Strain energy distribution in each layer of the laminated beam with eight fiber/matrix cells.

Fiber	E_i/E^*	$E_{ax,i}/E_{ax}^*$	$E_{s,i}/E_s^*$
1	0.113	0.053	0.005
2	0.113	0.053	0.006
3	0.114	0.053	0.006
4	0.114	0.053	0.006
5	0.114	0.053	0.006
6	0.114	0.053	0.006
7	0.113	0.053	0.006
8	0.113	0.053	0.005
matrix	0.093	0.579	0.953
	$E^* \times 10^1$ mJ	$E_{ax}^* \times 10^1$ mJ	$E_s^* \times 10^2$ mJ
Fibers + matrix	2.029	1.836	1.930

Table 14: Strain energy distribution in the eight fiber/matrix cells.

	FI* - MS		
	Cell	Fiber	Matrix
1	0.293	0.441	0.070
2	0.310	0.469	0.071
3	0.315	0.476	0.074
4	0.312	0.469	0.077
5	0.312	0.469	0.077
6	0.315	0.476	0.074
7	0.310	0.469	0.071
8	0.293	0.441	0.070

Table 15: Integral failure index over the eight fiber/matrix cells.

Figures
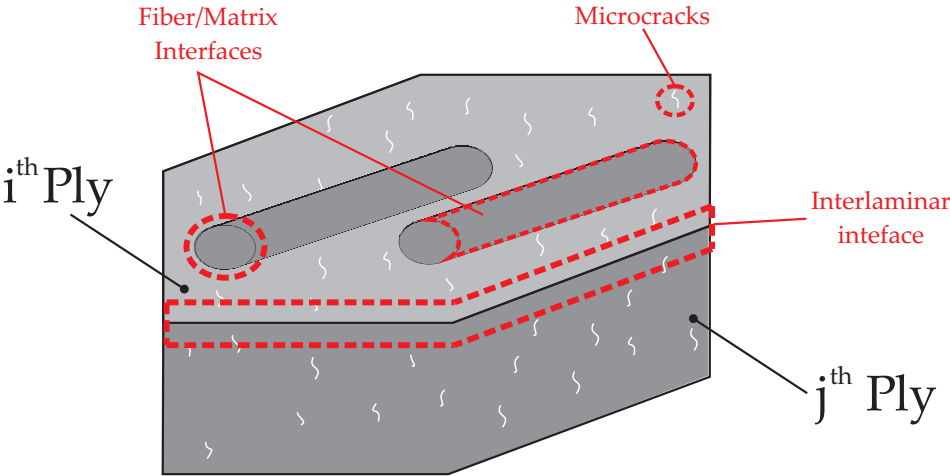
Figure 1: Integral sub-domains for the evaluation of failure parameters in composite structures.
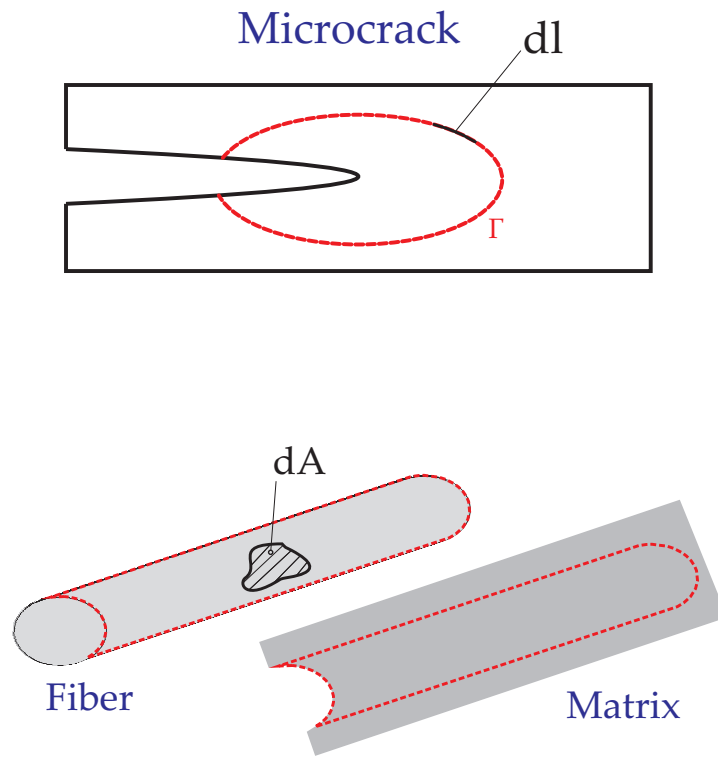
Figure 2: 1D-, 2D- and 3D-integral sub-domains.
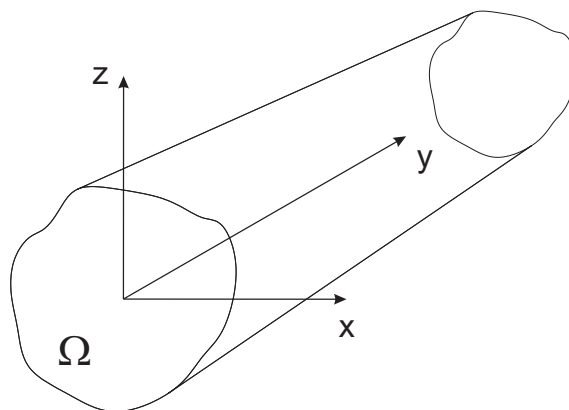
Figure 3: Coordinate frame.
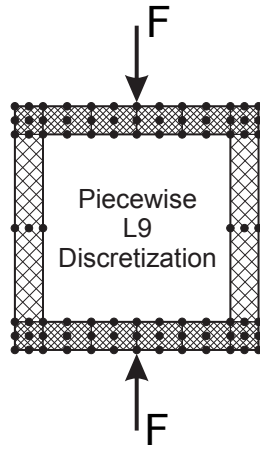
Figure 4: L9 element distribution above a cross-section undergoing local loads.
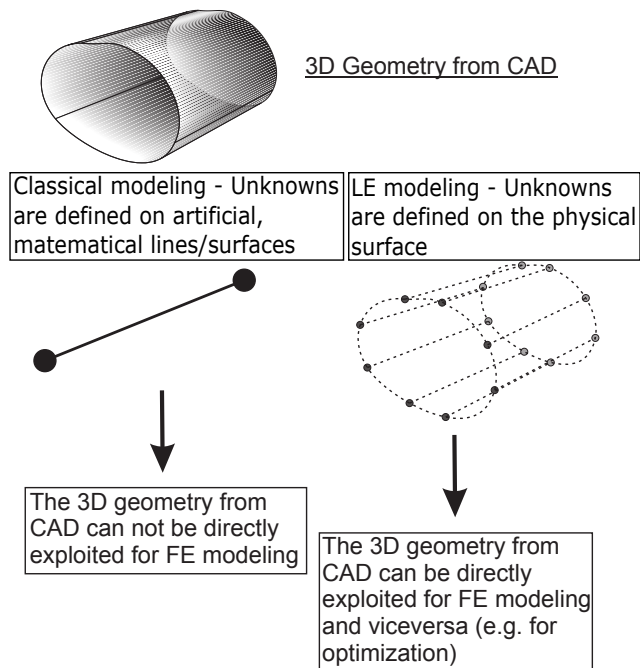
Figure 5: Classical and LE modeling strategies with respect to the 3D geometry.
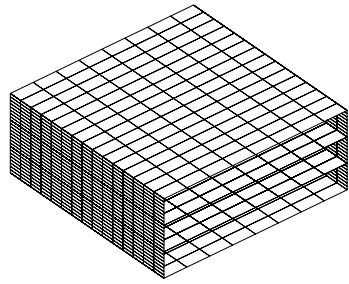
The three layers of the structure are the components of the CW
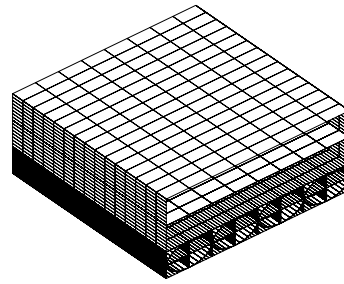
The top and middle layers, the fibers and matrix of the bottom layer are the components of the CW approach
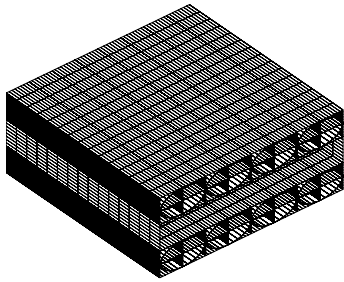
The middle layer, the fibers and matrix of the top and bottom layers are the components of the CW approach
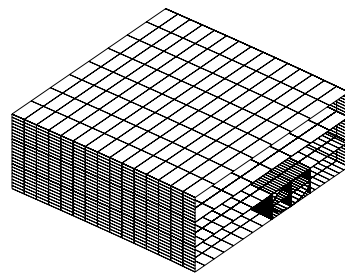
Only one fiber-matrix cell is embedded in the CW model

Figure 6: CW strategies for a fiber-reinforced structure.

Multicomponent Cross-Section
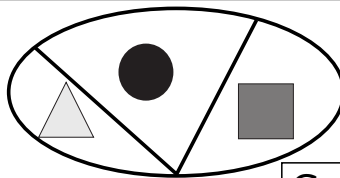
Component-Wise Element

Equivalent Single Component Element
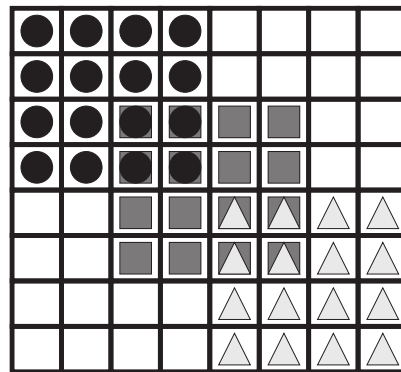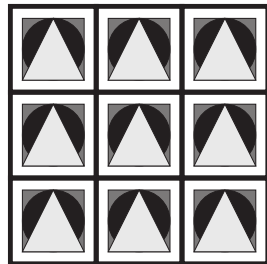
Figure 7: Stiffness matrix assemblage schemes.
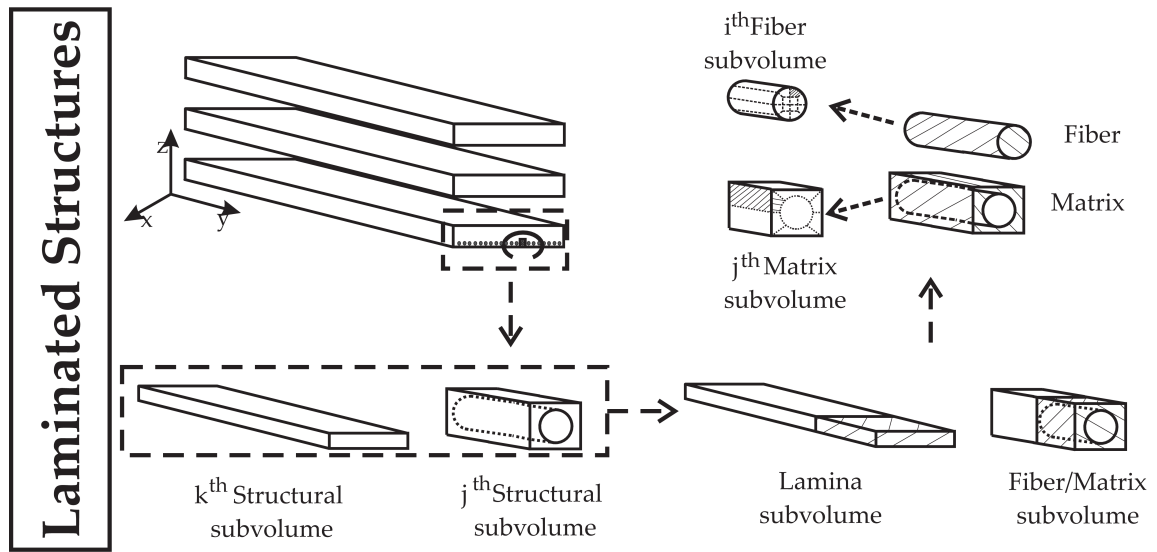
Figure 8: Examples of sub-volume distributions for a fiber reinforced composite plate.
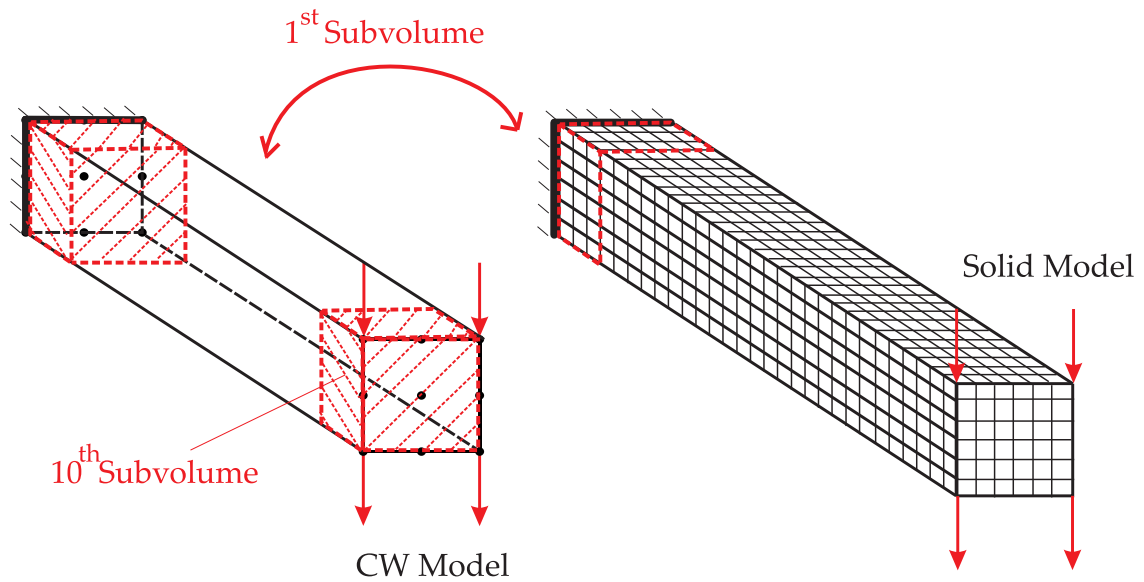
Figure 9: CW and Solid models for the homogeneous case.
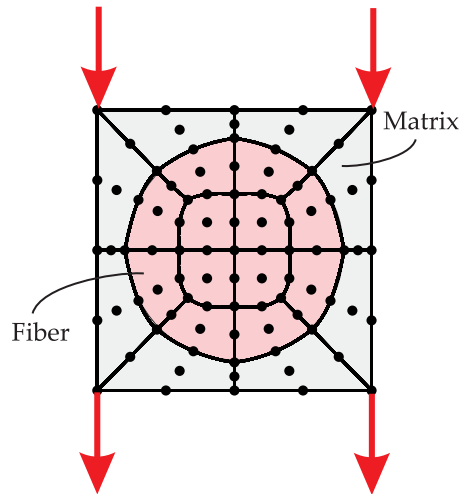
(a) Bending loading case
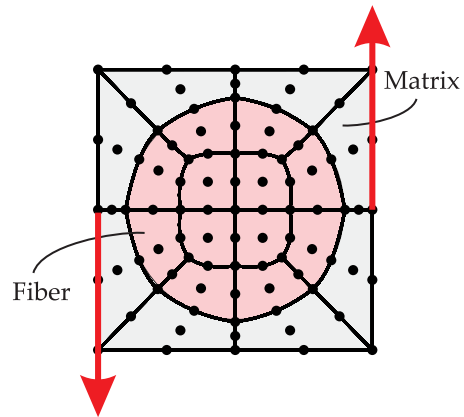
(b) Torsion loading case

Figure 10: Single cell loading cases and L9 distribution.

Failure Index - Maximum Stress

(a)

Failure Index - Tsai Wu
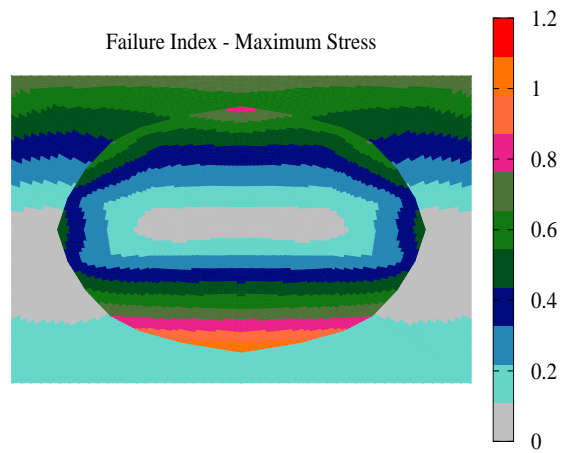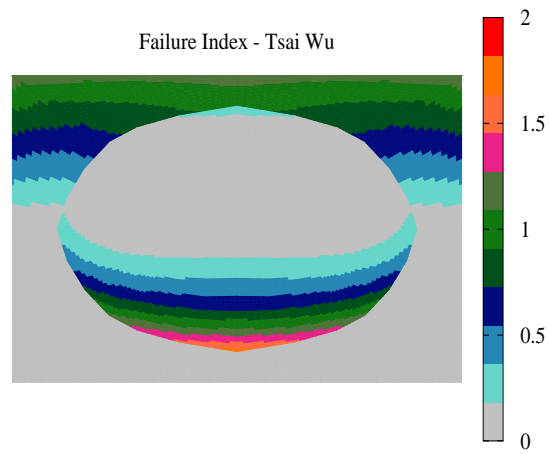
(b)

Figure 11: Maximum Stress (MS) and Tsai-Wu (TW) failure indexes over the single cell, clamped cross-section, bending loading.
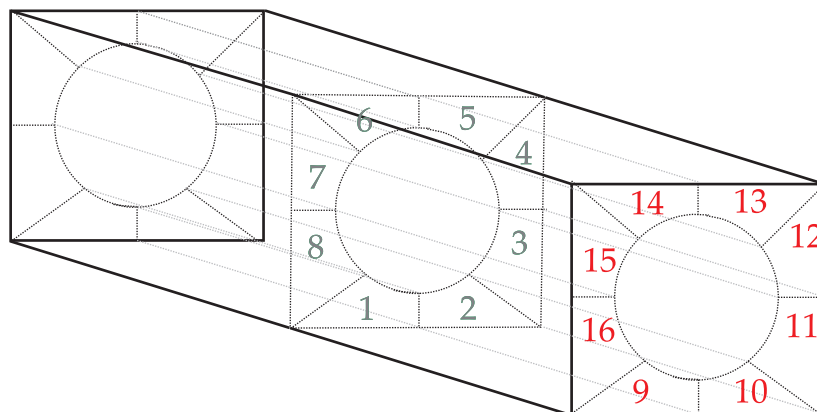

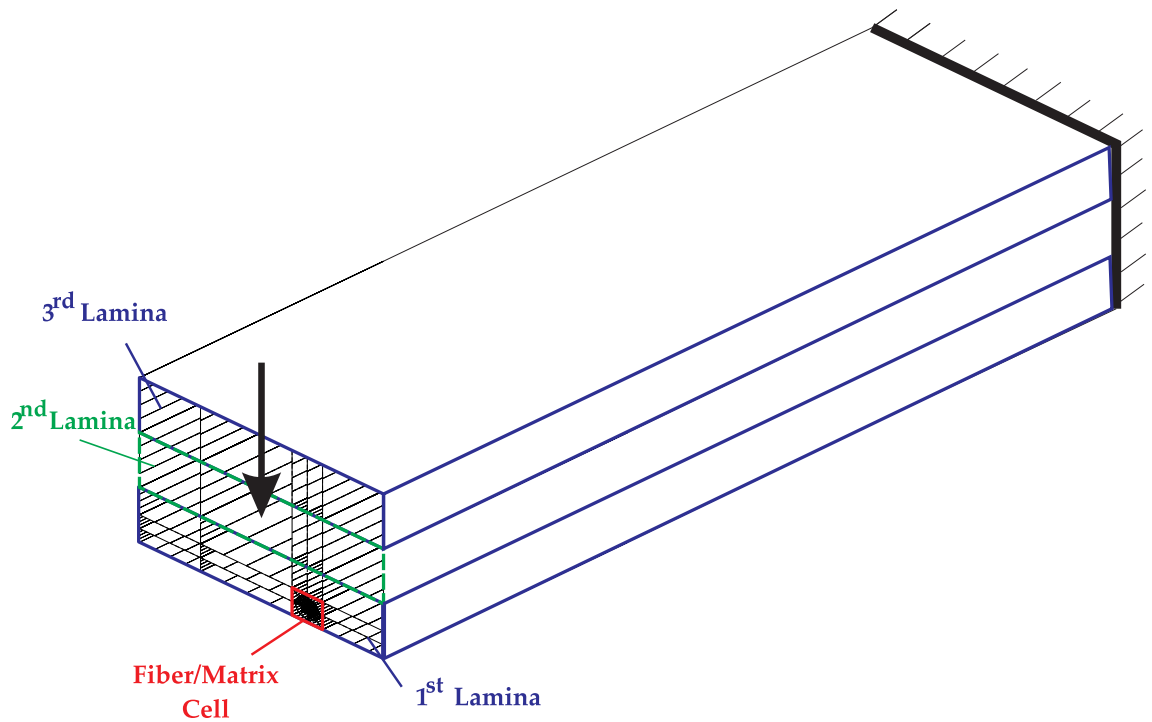Figure 12: Single cell matrix subvolumes near the free tip.

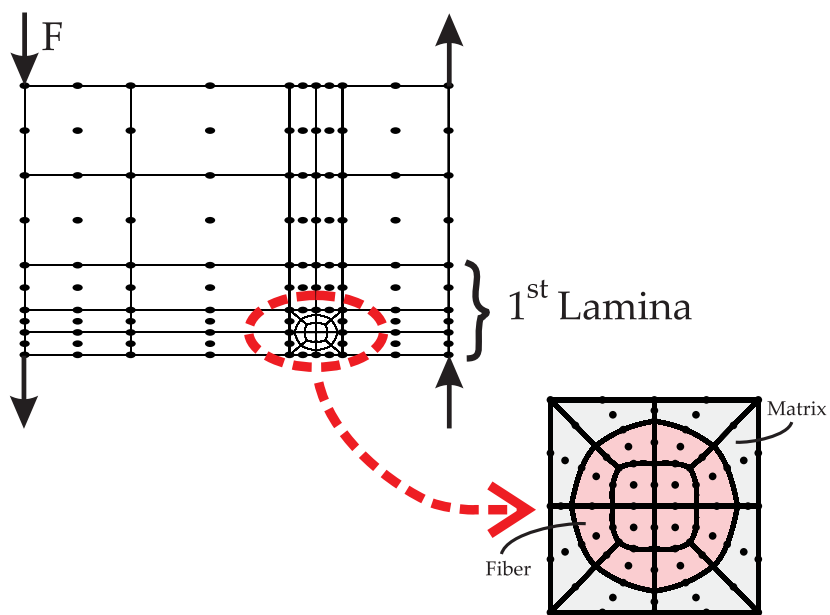Figure 13: Three-layer beam with a fiber/matrix cell and bending load.

Figure 14: Cross-section discretization of the three-layer beam with a fiber/matrix cell and torsional load, 41 L9.
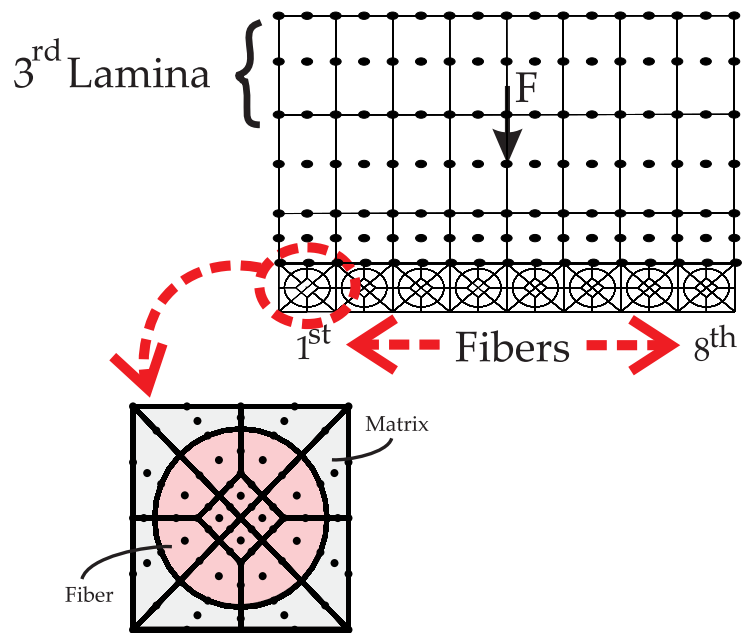
Figure 15: Cross-section discretization of the three-layer beam with eight fiber/matrix cells, 184 L9.